Title: Targeting aurora kinases with danusertib (PHA-739358) inhibits growth of liver metastases from gastroenteropancreatic neuroendocrine tumors in an orthotopic xenograft model

Authors: Katharina Fraedrich,[1] Jörg Schrader,[1] Harald Ittrich,[2] Gunhild Keller,[3] Artur Gontarewicz,[3] Verena Matzat,[1] Arno Kromminga,[4] Andrea Pace,[1] Jürgen Moll,[5] Michael Bläker,[1] Ansgar W. Lohse,[1] Dieter Hörsch,[6] Tim H. Brummendorf,[3,7] Daniel Benten[1]

[1]I. Medizinische Klinik, [2]Diagnostische und Interventionelle Radiologie, [3]II. Medizinische Klinik, Onkologisches Zentrum, Universitätsklinikum Hamburg-Eppendorf, Hamburg, Germany, [4]Labor Lademannbogen, Hamburg, Germany, [5]Nerviano Medical Sciences, Milan, Italy, [6]Zentralklinik Bad Berka, Germany, [7]IV. Medizinische Klinik, Universitätsklinikum Aachen, Germany

Running title: Danusertib in GEP-NETs

Keywords: aurora kinase inhibitor, histone H3, orthotopic, GEP-NET

Address for correspondence: Daniel Benten, MD, Universitätsklinikum Hamburg-Eppendorf, I. Medizinische Klinik, Martinistr. 52, 20246 Hamburg, Germany, Tel.: +49 40 7410 53910, Fax: +49 40 7410 58531, e-mail: d.benten@uke.de

Conflict of interest: J.M. is a former employee of Nerviano Medical Sciences, the manufacturer of danusertib. D.H. is a consultant and advisory board member of Novartis Pharma.

Tables: 3

Figures: 7

Abstract

Purpose: Aurora kinases play a crucial role in cell cycle control. Uncontrolled expression of aurora kinases causes aneuploidy and tumor growth. As conservative treatment options for advanced gastroenteropancreatic neuroendocrine tumors (GEP-NETs) are disappointing, aurora kinases may be an interesting target for novel therapeutic strategies. **Experimental Design:** Human GEP-NETs were tested for aurora kinase expression. The efficacy of new aurora kinase inhibitor danusertib was evaluated in two human GEP-NET cell lines (BON1 and QGP) in vitro and in vivo. **Results:** The majority of 10 insulinomas and all 33 non-functional pancreatic or midgut GEP-NETs expressed aurora A despite a mostly high degree of cell differentiation. Both human GEP-NET cell lines expressed aurora kinase A and B and high Ser10 phosphorylation of histone H3 revealed increased aurora B activity. Remarkably, danusertib led to cell cycle arrest and completely inhibited cell proliferation of the GEP-NET cells in vitro. Decreased phosphorlyation of histone H3 indicated effective aurora B inhibition. In a subcutaneous murine xenograft model, danusertib significantly reduced tumor growth in vivo compared to controls or mice treated with streptozotocine/5-fluorouracil. As a consequence, decreased levels of tumor marker chromogranin A were found in mouse serum samples. In a newly developed orthotopic model for GEP-NET liver metastases by intrasplenic tumor cell transplantation, dynamic magnetic resonance imaging proved significant growth inhibition of BON1 and QGP derived liver metastases. **Conclusions:** These results demonstrate that danusertib may impose a new therapeutic strategy for aurora kinase expressing metastasized GEP-NETs.

Translational Relevance

This study shows antitumoral activity of the novel aurora kinase inhibitor danusertib against GEP-NET growth in vitro and in vivo. Danusertib inhibits GEP-NET cell growth in association with cell cycle disruption and induction of apoptosis. The compound is effective at nanomolar concentrations in vitro, even below the level of inhibition of histone H3 phosphorylation. In addition, our data show that the antiproliferative activity of danusertib is higher compared with standard chemotherapy streptozotocine/5-fluorouracil, and the compound lowers an established tumor marker in vivo. Notably, since non-orthotopic in vivo models may not consider the relevant influence of tumor microenvironment, danusertib is also active toward GEP-NET liver metastases in a newly developed orthotopic cell transplantation model. These data indicate the potential use of danusertib for upcoming clinical investigation in patients with metastasized GEP-NETs.

Introduction

The incidence of neuroendocrine tumors of the gastroenteropancreatic system (GEP-NET) is increasing and more than 80% of patients are diagnosed in advanced stages, including the presence of liver metastases (1). Despite recent therapeutic improvements such as biotherapeutic regimens, targeted radiotherapy and locally ablative treatments (2-7), definitive cure in metastatic disease remains a rare event. Results from recent phase III studies using the mammalian target of rapamycin (mTOR) inhibitor everolimus or the multitargeted tyrosine kinase inhibitor sunitinib have shown for the first time, that molecular targeted therapy can successfully be applied in metastatic GEP-NETs (8). However, the clinical benefits attained in these studies were only moderate. Thus, novel therapeutic approaches for advanced stages of disease are clearly required.

Danusertib (formerly PHA-739358) is a small molecule, pan-Aurora kinase inhibitor (9). Aurora kinases are key regulators of protein phosphorylation during mitosis (10). These serin/threonine kinases interact with other proteins to control chromosome assembly and segregation. The aurora family of kinases, which consists of three members, aurora A, B, and C, differs in subcellular localization, kinetics of activation and function. Aurora kinases are frequently overexpressed in hematological malignancies and solid tumors (10, 11). Therefore, several aurora kinase inhibitors (AKI) have been developed and showed variable efficacy in different preclinical models (12, 13). The most advanced clinical compound is danusertib, a highly effective pan-AKI that inhibits aurora kinases A, B and C at nanomolar concentrations (9). Off-target effects of danusertib include inhibition of receptor tyrosine kinases such as Abl, Ret, FGFR-1 and TrkA. (9). Phase II clinical trials for patients with hematological malignancies and solid tumors are currently being carried out with this inhibitor.

The impact of aurora kinases for the tumorigenesis of GEP-NETs is largely unknown. First promising results were yielded by ZM447439, a selective aurora B kinase inhibitor used in

vitro at high concentrations (14). In order to further elucidate the applicability of aurora kinases in GEP-NETs as a potential target for anticancer therapy, we examined aurora-A expression in a series of GEP-NET tissue samples. The potential impact of aurora kinase inhibition in the treatment of GEP-NETs was evaluated using the novel small-molecule AKI danusertib. Its antiproliferative features and possible therapeutic mechanisms were examined in vitro and in a subcutaneous xenograft model. Based on the positive results, we developed a novel animal model for stable generation of GEP-NET liver metastases and could demonstrate in vivo efficacy of danusertib in this orthotopic tumor model.

Materials and Methods

Materials. Antibodies were for Ki-67, chromogranin A, (Dako, Hamburg, Germany), liver sinusoidal endothelial cells (LSEC) (Miltenyi, Bergisch Gladbach, Germany), CD31 (BD Biosciences, Heidelberg, Germany), aurora-A, aurora-B (Abcam, Cambridge, UK), phosphorylated histone H3 (Ser10), PARP (Cell Signaling Technology, Danvers, MA) and p21, p27, p53, proliferating cell nuclear antigen (PCNA) (Santa Cruz Biotechnology, Inc., Santa Cruz, USA). Danusertib was provided by Nerviano Medical Sciences (Milan, Italy) and dissolved in dimethyl sulfoxide (DMSO). The final DMSO concentration for all in vitro assays was 0.1%. For in vivo experiments, an in situ salt was mixed as described (15).

Immunohistochemistry of human GEP-NET. Formalin-fixed, paraffin embedded tissue samples of surgically resected human insulinomas, non-functional pancreatic NETs and midgut NETs from small intestine were pretreated, immunostained and analyzed as described (12, 15).

Human GEP-NET cells and culture. Serotonin secreting human pancreatic carcinoid cell line BON1 and human nonfunctioning pancreatic islet cell tumor line QGP (16) were maintained in Dulbecco's modified Eagle's medium (DMEM) containing 10% fetal calf serum,

100 units/ml penicillin and 10 µg/ml streptomycin at 37°C in a 5% CO2 atmosphere.

Cell analysis, immunostaining, and flow cytometry. Cells were seeded in DMEM, fixed and immunostained for aurora-A, aurora-B and histone H3 phosphorylation, as described (12). For analysis of cell proliferation, increasing concentrations of danusertib (dissolvent control; 5nM−5µM) were added after 24h of cell culture. 48−120h later, the number of viable cells was determined (12). Analysis of DNA content and H3 phosphorylation were performed by flow cytometry as described (12, 13, 17).

Western Blot. Tumors resulting after subcutaneous transplantation of BON1 and QGP cells were shredded in Tissue Protein Extraction Reagent (Pierce Biotechnology, Inc., Rockford IL) followed by homogenization with 3x5 s sonication. Total proteins from treated cells and untreated controls were extracted as described (12). Nuclear extracts were prepared by sequential cell lysis using the non-denaturating detergent Igepal (Sigma), followed by centrifugation and lysis of the nuclei-containing pellet with a hypertonic buffer containing 0.4M NaCl. 30µg Protein extract was loaded on SDS-PAGE (12% gel) and electrotransferred. Immunodetection was carried out as described (18), using the following antibodies: PARP, phospho-AKT, phospho-JNK, p53, p21, p27, Actin, p-Erk.

Animals. The Special Animal Core of the Hamburg University Medical Center provided 6- to 10-week old non-obese diabetic/severe combined immunodeficiency (NOD/SCID) mice. All animal experiments were approved by the local authorities in accordance with the NIH Guide for Care and Use of Laboratory animals.

Subcutaneous tumor xenografts. To generate subcutaneous tumors, $5x10^6$ BON1 or QGP cells in 0.1mL DMEM containing 2% FCS were mixed with extracellular matrix gel (12) and injected into flanks of NOD/SCID mice. Treatment was initiated when tumor volumes reached median sizes of 22-126 mm^3. Determination of tumor size, assignment of mice to

treatment groups, termination criteria and tumor sampling has been described previously (12).

Orthotopic model of GEP-NET liver metastases. To generate GEP-NET liver metastases, the spleen was exposed by a small flank laparotomy. $0.5x10^6$ BON1 or QGP cells were injected in 0.2ml DMEM containing 2% FCS using 27-gauge needles. Hemostasis was secured by ligature of the splenic pole. Splenectomy was performed the 10min following cell injection to prevent growth of tumor cells inside the spleen. In pilot experiments for biodistribution of tumor cells, direct cell transplantation into the portal vein was also used. Magnetic resonance imaging (MRI) of transplanted mice was performed weekly to detect liver metastases following tumor cell transplantation.

Identification of human cells in mice. To identify transplanted GEP-NET cells in organs, liver lobes, lungs, kidneys, heart and intestine were collected 2 hours after cell injection and DNA-PCR for human specific centromere regions was performed (19). Transplanted human cells were identified with in situ hybridization (digoxigenin-labeled pancentromeric probe) as described previously (19), with the following modification: to visualize hybridization signals, sections were incubated with FITC-conjugated anti-digoxigenin Fab fragments for 1h at room temperature. Immunohistochemistry of xenograft tumors was performed as described previously (12), with the following primary antibodies: aurora-A and -B (1:250), Chromogranin A (1:400), Ki-67 (1:50), PCNA (1:500), CD31 (1:50) and LSEC (1:500).

Magnetic resonance imaging. MR measurements of xenografted mice were performed on 4-day intervals for volumetric analysis. Mice were imaged with a 3 Tesla Scanner (Intera, Philips Medical Systems, Best, The Netherlands) using a custom-made small solenoid animal coil (Philips Research Laboratories, Hamburg, Germany). We applied a T2-weighted 2D turbo spin echo sequence (TR/TE 3820/98 ms, 30x30 mm field of view (FoV), matrix 144x140, 20 slices, slice thickness 1.0 mm, effective voxel volume ($0.20mm^3$), acquisition time 2:32 minutes), in

transversal adjustment. During MRI procedures, animals were anesthetized with Ketamin/Xylazin. Volumetric quantification of liver metastases was performed by computer-aided software (ImageJ 1.37v, National Institutes of Health, USA).

Experimental protocol. Mice bearing BON1 or QGP tumors were divided into a treatment group receiving danusertib intraperitoneally (i.p.) at a dose of 2x15 mg/kg/d or a control group receiving the same volume of vehicle solution (5% dextrose). Streptozotocine and 5-fluorouracil were applied i.p. at a dose of 1x15mg/kg/d.

Chromogranin A serum levels. For chromogranin A (CgA) serum analysis, blood was collected at the end of each BON-1 experiment. CgA serum levels were measured with an enzyme-linked immunosorbent assay (Maier Analytik, Sinsheim, Germany) according to the manufacturer's instructions.

Statistical methods. Where applicable (see below), significance of differences was analyzed by χ^2 tests, Fisher's exact test, or two-tailed Student's t-tests. P values <0.05 were considered significant.

Results

Expression of aurora kinases and phospho-H3S10. 43 human GEP-NET samples were available for analysis of aurora kinase expression (10 insulinomas, 13 non-functional pancreatic NETs, 20 mid-gut NETs from small intestine) most of which were grade 1 and 2 (Table 1). Aurora-A was expressed in 8/10 insulinomas, and in all non-functional pancreatic and midgut NETs (Fig. 1A, Table 1), whereas surrounding non-malignant tissue and controls (normal pancreas) were negative (data not shown). Aurora-B was not expressed in insulinomas, whereas 2/13 non-functional pancreatic NETs (1x G1, 1x G3) and 3/20 midgut NETs (2x G1, 1x G2) expressed aurora B (Fig. 1B, Table 1). 4/5 aurora-B positive GEP-NETs also expressed down stream target histone H3, which is phosphorylated at Ser10 (phospho-H3S10) by aurora-B during

mitosis (Table 1).

Serotonin secreting human pancreatic carcinoid cell line BON1 and human nonfunctioning pancreatic neuroendocrine tumor line QGP were tested positive for aurora-A and aurora-B by Western blot (Fig. 1C). Differential cell lysis revealed primarily nuclear localization. The overall expression of both aurora kinases was higher in BON1 compared to QGP cells, which is in line with higher expression of the proliferation marker PCNA (Fig. 1C). Aurora kinase expression was confirmed in subcutaneous tumors after xenotransplantation of both human cell lines into immunodeficient mice (Fig. 1D-E).

Phospho-H3S10 was expressed in both GEP-NET cell lines: quantitative analysis of phospho-H3S10 by flow cytometry revealed a cell fraction of 1.60±0.04% in BON1, and 1.49±0.04% in QGP cells, indicating aurora-B activity in both human GEP-NET cell lines. Phospho-H3S10 expression was also confirmed by immunostaining of subcutaneous xenograft tumors (Fig. 1F).

Inhibition of tumor cell proliferation by danusertib. Cell counting analysis with trypan blue exclusion assay using different concentrations of the compound showed that danusertib, starting from 50nM, led to a complete stop of GEP-NET cell proliferation in BON1 cells and to a decrease of cell numbers in QGP cells (Fig. 2A and 2B; $p<0.001$ for both cell lines at 96h). Flow cytometric cell cycle analysis revealed a dose dependent effect of danusertib (Fig. 2C). Significant reduction of cells in S-phase started from 50nM, leading to endoreduplication of cells with a substantial increase of the DNA content (4N and >4N fractions) and to a complete block of mitosis with loss of the 2N fraction, at higher concentrations (Fig 2C). Phosphorylation of the aurora-B downstream target H3S10 was effectively inhibited in both GEP-NET cell lines following treatment with danusertib (Fig. 2D for BON1). However, as observed in other cell lines (12), a significant inhibition of H3S10 phosphorylation started at concentrations 10-fold higher

than the dose inhibiting proliferation (phospho-H3S10 cell fraction at 500nM: BON1: 0.05% vs. 1.63% in controls, $p<0.01$; n=3; QGP: 0.03% vs. 1.49%, $p<0.01$; n=3).

Western Blot of cell lysates treated for 48h with danusertib at various concentrations showed an increase of poly [ADP-ribose] polymerase 1 (PARP-1) cleavage upon treatment indicating induction of apoptosis (Fig 2E). Maximal PARP-1 cleavage was observed at 50nM in both cell lines, whereas higher doses resulted in a gradual decrease down to baseline at the highest dose of 5µM. There was no apparent effect of the treatment on either p53 accumulation or p21 expression; similarly, we did not observe an increase in the G1 transition cell cycle regulator p27 (data not shown). To rule out any off-target effects of danusertib on other mitogenic signaling pathways, the activation of PI3K/Akt and MAPK pathways was analyzed. However, danusertib did not affect basal activities or fetal calf serum induced activation of Akt, Erk and JNK in both cell lines (data not shown).

Danusertib treatment inhibits growth of subcutaneous GEP-NET xenografts and lowers serum chromogranin levels. Treatment of tumor bearing mice with danusertib at a dose of 2x15 mg/kg/d decreased growth of BON1 and QGP xenografts (Fig. 3A-B). BON1 tumor growth was significantly inhibited from day 4 ($p<0.001$) until the end of the experiment ($p<0.001$). The mean absolute tumor volume was reduced by 88.2%, and the mean percental tumor growth was also reduced by 88.2%, compared to vehicle treated controls (Fig. 3A, Table 2). In mice with QGP xenografts, treatment with danusertib led to a virtual shrinkage of QGP tumors from day 4 ($p<0.001$) until the end of the experiment ($p<0.001$). The final tumor volume was only 6.3±8.2% of the original tumor volume (Fig. 3B, Table2). Mean absolute and percental tumor growth in danusertib treated mice was reduced by 98.4% and 98.6%, respectively compared to vehicle treated controls. When compared to treatment with streptozotocine/5-fluoruracil (STZ/5-FU), which is a frequently used cytostatic therapy for GEP-NETs, the

antiproliferative effect of danusertib was significantly higher from day 12 ($p<0.001$) in both BON1 and QGP tumors (Fig. 3A-B, Table 2).

In serum analyses of BON1 tumor bearing mice, we detected elevated levels of the clinically applied GEP-NET tumor marker chromogranin A (CgA). The average serum level was 23±15nmol/l after 2 weeks (untransplanted controls <4 nmol/l) and rose to 47.3±22.7nmol/l in untreated animals at the end of experiments ($n=16$; $p<0.001$). CgA levels were significantly lower in Danusertib treated animals (12.0±12.4nmol/l) compared to vehicle treated controls ($p<0.001$, $n=9$) and mice treated with STZ/5-FU (32.0±12.9nmol/l, $p<0.05$, $n=6$) (Fig. 3C). Despite low-level expression of CgA in QGP cells by Western blotting, we were not able to detect CgA in the serum of QGP tumor-bearing mice.

Biodistribution of GEP-NET cells in intact animals for generation of an orthotopic model of liver metastastes. Based on successful inhibition of tumor growth in subcutaneous xenografts, we next aimed to generate an orthotopic in vivo model to evaluate the effects of danusertib on GEP-NET liver metastases. To identify differences in organ-specific targeting, we injected BON1 or QGP cells into the portal vein or the spleen followed by sequential splenectomy in NOD-SCID mice. Both injection routes led to rapid translocation of cells into the liver within 2 hours, as verified by human specific CMT1 PCR. A faint PCR signal was also found in the lungs and the intestine, whereas the human sequence was absent in kidneys, and heart (Fig. 4A). After 4 weeks, multiple tumor nodules were detected in the liver and a massive hepatomegaly had occurred (Fig. 4B). To visualize GEP-NET cells in tissues, we used fluorescence-in-situ-hybridization for human specific sequences, which verified that tumor nodules in the liver were comprised of cells of human origin (Fig. 4C). By in-situ-hybridization, we found no evidence of transplanted human tumor cells in other organs, including the lungs. Histology of livers showed multiple tumors comprised of small cells with a necrotic area in the

center of the nodule (Fig. 4D).

Characterization of liver metastases from GEP-NET cells. BON1 liver metastases showed strong expression of CgA by immunohistochemistry (Fig. 5A), indicating that cells retained their in vitro characteristics of neuroendocrine differentiation. BON1 cells showed extensive proliferation in vivo, as demonstrated by immunohistochemistry for Ki-67 and PCNA (Fig. 5B-C). Tumors derived from nonfunctioning pancreatic islet cell tumor derived QGP cells were negative for chromogranin A but liver metastases from these cells retained typical NET morphology; e.g. small cells with a high nucleus/cytoplasm ratio (Fig. 5D). Human origin of these metastases was verified by in-situ-hybridization (Fig. 5E). Although QGP cells proliferated less extensively, the proliferative index in both cell lines was >20% in metastases in all animals (data not shown). Capillary vessels in human GEP-NET metastases were of murine origin as verified by immunohistochemistry using mouse specific antibodies for CD31 or liver sinusoidal endothelial cells, indicating tumor angiogenesis from the host liver (Fig. 5F).

Treatment of GEP-NET liver metastases with danusertib. To identify the time course of metastatic tumor growth, we performed magnetic resonance imaging of recipient mice and tumor volumetry. 2-3 weeks after cell transplantation, small metastatic tumor nodules (diameter 100-120µm) in the liver became detectable with a metastatic tumor take rate of approximately 80% for both transplanted cell lines. BON1 metastases grew more diffusely from small originating tumor nodules, whereas QGP metastases showed a different growth pattern dominated by singular tumor nodules (Fig. 6A and B).

In transplanted mice, treatment with danusertib or vehicle was commenced when liver metastases became clearly detectable and were eligible for volumetric analysis, which was after 2-3 weeks following cell transplantation. Average size of BON1 metastases (single nodules) before treatment was $2.9\pm1.3mm^3$ (n=20). While liver metastases of BON1 tumors in vehicle-

treated controls continued to grow until large areas of the liver were replaced by tumor tissue, treatment with danusertib significantly inhibited growth of liver metastases (day 12 after start of treatment 55.9±39.7mm^3, n=10 vs. 5.2±3.8mm^3; n=10; $p<0.01$) (Fig. 6A and 6C, Table 3). This corresponds to a relative tumor volume compared to day 0 (100%) of 1495.3±1277.9% in controls vs. 164.5±50.2% in danusertib treated mice ($p<0.01$). Mean absolute and percental tumor growth in danusertib treated mice was reduced by 90.7% and 89.0%, respectively compared to vehicle treated controls. Average size of QGP metastases in the liver before treatment was 6.8±3.7mm^3 (n=9). Danusertib entirely inhibited growth of QGP metastases, although no shrinkage was observed, as in subcutaneous tumors (control: day 12 51.7±35.0mm^3; n=4 vs. danusertib 6.1±4.3mm^3; n=5 $p<0.05$) (Fig. 6B and 6C, Table 3). This corresponds to a relative tumor volume of 810.7±355.4% vs. 108.7±58.9%, $p<0.01$. The mean absolute tumor volume was reduced by 88.2%, and the mean percental tumor growth was reduced by 86.6%, compared to vehicle treated controls.

Discussion

Metastatic GEP-NETs are currently managed with standard chemotherapies, such as STZ/5-FU for differentiated tumors of pancreatic origin and platinum-based protocols for undifferentiated GEP-NETs with poor efficacy. Although two recent landmark studies have demonstrated for the first time, that targeted therapy is effective in GEP-NETs (20, 21), the overall effects remain moderate and non-response to the substances emphasizes the demand for alternative strategies.

Overexpression of aurora kinases has been demonstrated in many tumors. Thus, the inhibition of aurora kinases moved into the focus of anticancer therapy (22-25). Since their role has never been assessed in GEP-NETs, we first screened expression in human insulinomas, non-functional pancreatic NETs and midgut NETs. While aurora-A was highly abundant in these

tumors, aurora-B expression was enhanced in only five cases. In contrast, in both human GEP-NET cell lines, with high proliferative indices in xenograft models, both aurora A and aurora B were expressed. This may be due to the differentiation of human GEP-NETs analyzed and may not reflect the situation in higher proliferative metastatic tumors. This also points out limitations of existing models since all available human GEP-NET cell lines have high proliferative indices. Alteration of aurora-B controlled cellular mechanisms leads to aneuploidy, one of the main features and driving forces of cancer progression. Furthermore, overexpression of aurora-B has been observed in several tumor types, and has been linked with poor prognosis of cancer patients (24). Only one of our 43 GEP-NETs was a highly proliferative grade 3 tumor. Although this tumor was indeed positive for aurora-B and histone H3, the other 4 NETs with these properties were grade 1 or 2. Therefore, whether aurora-B expression is also related to malignant progression of GEP-NETs into higher proliferative tumors needs to be investigated with a larger number of clinical tumor specimens of various grades and proliferative indices. On the other hand, we detected a strong antiproliferative effect of danusertib already at low concentrations, while aurora-B inhibition –revealed by decreased phosphorylation of histone H3– only appeared at higher concentrations. Therefore, the effect of cell cycle inhibition and endoreduplication at low concentrations without measurably affecting histone H3 most likely results from successful aurora-A inhibition with aurora-A regulated spindle apparatus being the primary target. This effect has recently been observed in hepatocellular carcinoma models and is in accordance with quantitative kinase inhibition assays showing higher sensitivity of aurora-A for danusertib (12).

Recently, Georgieva and colleagues reported first promising in vitro results using high doses of aurora-B kinase inhibitor ZM447439 (14). To our knowledge, no clinical trial activity is being pursued with this compound. In contrast, pan-aurora kinase inhibitor danusertib is in advanced clinical development. Thus, a phase I clinical trial evaluating danusertib in 50 patients

with metastatic solid tumors mostly derived from the gastrointestinal tract, has been completed in 2009 (26). Stable disease was observed in 24% of patients. In ongoing phase II clinical trials the efficacy of danusertib is evaluated in patients suffering from tumor entities resistant to first or second line chemotherapy (27-29).

In the present study we demonstrate for the first time that aurora kinases can successfully be targeted in GEP-NETs in vivo. Efficacy of danusertib was documented in human GEP-NET cells and tumor xenografts and resulted in inhibition of proliferation and tumor growth. Mechanisms of action included cell cycle arrest and apoptosis. However, only in QGP tumors a reduction of tumor size could be attained while the size of BON1 tumors size remained stable during treatment. Interestingly, the selective aurora B inhibitor ZM447439 showed strong induction of apoptosis in the same cell lines (14). This may be due to the high concentrations at micromolar ranges applied in the in vitro experiments. Most probably, these concentrations cannot be reached in vivo. However, as no in vivo studies were performed with ZM447439 currently no statement concerning the effect of the inhibitor at lower concentrations can be made (14). The reason that apoptosis induction was demonstrated mainly at lower concentrations of danusertib may be related to the ongoing cell cycle activity shown by detectable S-phase at 50nM. In contrast, we observed a massive reduction in S-phase at higher doses, consecutively leading to reduced apoptosis. It is therefore likely that danusertib-induced apoptosis is dependent on actively dividing cells. Treatment with concentrations of 500nM resulted in a significantly reduced phosphorylation of histone H3, resulting in a complete block of mitosis and loss of the 2N fraction. Remarkably, such serum concentrations are also achievable in humans (30).

Whereas BON1 tumors remained stable under danusertib treatment, subcutaneous QGP tumor sizes decreased. These in vivo results reflect in vitro experiments with decreased cell numbers only in QGP cells, although apoptosis was observed in both cell lines. This may be due

to the higher proliferation rate in BON1 cells leading to a compensatory increase in cell numbers. Interestingly, reduced cell proliferation and tumor reduction occurred early in the treatment phase, and remained stable thereafter. Cells with normal 2N chromosome numbers may be more susceptible to apoptosis than cells with higher >2N chromosome numbers after endoreplication. Alternative mechanisms, such as differences in cell cycle analyses or the p53/p21 axis could not be detected. Since various receptor tyrosine kinases that might have been influenced by danusertib share the same mitogenic signaling cascades as a mechanism of action, off-target effects of the compound were ruled out by showing unaltered Erk (downstream target of Ras/Raf signaling, FGFR, src), JNK (several growth factors, cell surface receptors, src) and Akt (PI-3 Kinase, FGFR).

Although we were able to show reductions in tumor growth after treatment with danusertib, the use of a heterotopic in vivo system may not reflect the influence of the relevant tumor microenvironment, an important factor in tumor growth and metastasis (31, 32). Since liver metastases constitute the main clinical problem in GEP-NETs, the present study extends the established knowledge of antitumor effects and mechanisms of danusertib in an orthotopic model of metastatic GEP-NETs. In accordance, an interesting orthotopic tumor model has recently been established to combine somatostatin receptor szintigraphy with MRI after injection of rat-derived pancreatic tumor cells into mouse pancreas (33). In our model, liver metastases derived from human GEP-NET cell lines retained characteristics of the GEP-NETs, i.e. CgA expression and secretion as well as stimulation of angiogenesis. Generation of liver metastases was achieved by techniques used in therapeutic liver cell transplantation, e.g. intrasplenic or intraportal injection (15, 34). In line with the metastatic spread observed in gastrointestinal cancer, tumor cells enter the liver sinusoids via the portal venous blood. With regard to the increasing knowledge about the importance of tumor-stroma interactions (31), this enables analysis of treatment efficacy on

tumor cell growth under similar conditions as in human disease. Furthermore, the understanding of tissue-specific pharmacological properties of danusertib may play an important role to predict the response of metastases at similar anatomical sites in humans (32, 35). Thus, tumor shrinkage of QGP cells occurred in the subcutaneous tumor model whereas in the orthotopic model, only stable disease was obtained. We also observed a more rapid tumor growth of liver metastases compared to the subcutaneous model. This may be due to a stimulatory effect of the liver microenvironment e.g. the presence of growth factors such as IGF1 (36). Therefore, this new model offers options for translational research with potential clinical relevance. Furthermore, we were recently able to demonstrate that BON1 cells are amenable for multicolor labeling by simultaneous lentiviral transduction with three fluorescence proteins, which remained stable after xenografting (37). This technique, together with intrahepatic formation of liver metastases for serial MR-imaging will offer new opportunities to study clonality of GEP-NETs and mechanisms of chemotherapy resistance.

As demonstrated by several studies, circulating CgA correlates with tumor burden and prognosis in humans (38-40) and has a high diagnostic accuracy (41). We observed significantly decreased CgA levels in danusertib treated mice compared to controls, and standard therapy with STZ/5-FU. However, in line with a previous study we observed a large variety of CgA levels in tumor bearing animals before treatment (42). Furthermore, CgA levels did not correlate with the reduction in tumor mass observed in treated mice. Thus, CgA levels may not be a mere reflection of tumor mass, but other mechanisms regulating CgA release from tumor cells may play a role in different treatment modalities. Whether CgA could act as a biomarker for therapy monitoring and outcome needs to be studied further. It also needs to be evaluated if AKI have the same positive effect on pancreatic NETs as the recently approved everolimus and sunitinib which had been shown to delay tumor growth using a murine transgenic pancreatic islet-cell tumor model (20,

21).

In conclusion, the current study supports aurora kinase targeting using potent small-molecule inhibitors such as danusertib for the treatment of GEP-NETs. Our study advances previous work by demonstrating strong antitumor activity in a new orthotopic tumor model of GEP-NET liver metastases. The potent effects on cell cycle interference and apoptosis induction provide rationales for forthcoming clinical trials targeting aurora kinases in GEP-NETs.

Grant Support

This work was partially supported by Grant Numbers BE2559/2-1 and SFB 841 C7 from Deutsche Forschungsgemeinschaft (DB) and Forschungsförderungsfonds Medizin, Hamburg University (DB, GK)

References

1. Modlin IM, Oberg K, Chung DC, Jensen RT, de Herder WW, Thakker RV, et al. Gastroenteropancreatic neuroendocrine tumours. Lancet Oncol. 2008;9:61-72.

2. Fazio N, Cinieri S, Lorizzo K, Squadroni M, Orlando L, Spada F, et al. Biological targeted therapies in patients with advanced enteropancreatic neuroendocrine carcinomas. Cancer Treat Rev. 2010;36 Suppl 3:S87-94.

3. Hellman P, Ladjevardi S, Skogseid B, Akerstrom G, Elvin A. Radiofrequency tissue ablation using cooled tip for liver metastases of endocrine tumors. World J Surg. 2002;26:1052-6.

4. Henn AR, Levine EA, McNulty W, Zagoria RJ. Percutaneous radiofrequency ablation of hepatic metastases for symptomatic relief of neuroendocrine syndromes. AJR Am J Roentgenol. 2003;181:1005-10.

5. Kwekkeboom DJ, de Herder WW, Krenning EP. Somatostatin receptor-targeted radionuclide therapy in patients with gastroenteropancreatic neuroendocrine tumors. Endocrinol Metab Clin North Am. 2011;40:173-85, ix.

6. Nicolas G, Giovacchini G, Muller-Brand J, Forrer F. Targeted radiotherapy with radiolabeled somatostatin analogs. Endocrinol Metab Clin North Am. 2011;40:187-204, ix-x.

7. Ruszniewski P, O'Toole D. Ablative therapies for liver metastases of gastroenteropancreatic endocrine tumors. Neuroendocrinology. 2004;80 Suppl 1:74-8.

8. Turaga KK, Kvols LK. Recent progress in the understanding, diagnosis, and treatment of gastroenteropancreatic neuroendocrine tumors. CA Cancer J Clin. 2011;61:113-32.

9. Gontarewicz A, Brummendorf TH. Danusertib (formerly PHA-739358)--a novel combined pan-Aurora kinases and third generation Bcr-Abl tyrosine kinase inhibitor. Recent Results Cancer Res. 2010;184:199-214.

10. Keen N, Taylor S. Aurora-kinase inhibitors as anticancer agents. Nat Rev Cancer. 2004;4:927-36.

11. Warner SL, Munoz RM, Stafford P, Koller E, Hurley LH, Von Hoff DD, et al. Comparing Aurora A and Aurora B as molecular targets for growth inhibition of pancreatic cancer cells. Mol Cancer Ther. 2006;5:2450-8.

12. Benten D, Keller G, Quaas A, Schrader J, Gontarewicz A, Balabanov S, et al. Aurora kinase inhibitor PHA-739358 suppresses growth of hepatocellular carcinoma in vitro and in a xenograft mouse model. Neoplasia. 2009;11:934-44.

13. Lens SM, Voest EE, Medema RH. Shared and separate functions of polo-like kinases and aurora kinases in cancer. Nat Rev Cancer. 2010;10:825-41.

14. Georgieva I, Koychev D, Wang Y, Holstein J, Hopfenmuller W, Zeitz M, et al. ZM447439, a novel promising aurora kinase inhibitor, provokes antiproliferative and

proapoptotic effects alone and in combination with bio- and chemotherapeutic agents in gastroenteropancreatic neuroendocrine tumor cell lines. Neuroendocrinology. 2010;91:121-30.

15. Benten D, Kumaran V, Joseph B, Schattenberg J, Popov Y, Schuppan D, et al. Hepatocyte transplantation activates hepatic stellate cells with beneficial modulation of cell engraftment in the rat. Hepatology. 2005;42:1072-81.

16. Grabowski P, Schrader J, Wagner J, Horsch D, Arnold R, Arnold CN, et al. Loss of nuclear p27 expression and its prognostic role in relation to cyclin E and p53 mutation in gastroenteropancreatic neuroendocrine tumors. Clin Cancer Res. 2008;14:7378-84.

17. Gontarewicz A, Balabanov S, Keller G, Colombo R, Graziano A, Pesenti E, et al. Simultaneous targeting of Aurora kinases and Bcr-Abl kinase by the small molecule inhibitor PHA-739358 is effective against imatinib-resistant BCR-ABL mutations including T315I. Blood. 2008;111:4355-64.

18. Huber S, Schrader J, Fritz G, Presser K, Schmitt S, Waisman A, et al. P38 MAP kinase signaling is required for the conversion of CD4+CD25- T cells into iTreg. PLoS One. 2008;3:e3302.

19. Benten D, Cheng K, Gupta S. Identification of transplanted human cells in animal tissues. Methods Mol Biol. 2006;326:189-201.

20. Raymond E, Dahan L, Raoul JL, Bang YJ, Borbath I, Lombard-Bohas C, et al. Sunitinib malate for the treatment of pancreatic neuroendocrine tumors. N Engl J Med. 2011;364:501-13.

21. Yao JC, Shah MH, Ito T, Bohas CL, Wolin EM, Van Cutsem E, et al. Everolimus for advanced pancreatic neuroendocrine tumors. N Engl J Med. 2011;364:514-23.

22. Jeng YM, Peng SY, Lin CY, Hsu HC. Overexpression and amplification of Aurora-A in hepatocellular carcinoma. Clin Cancer Res. 2004;10:2065-71.

23. Li D, Zhu J, Firozi PF, Abbruzzese JL, Evans DB, Cleary K, et al. Overexpression of oncogenic STK15/BTAK/Aurora A kinase in human pancreatic cancer. Clin Cancer Res. 2003;9:991-7.

24. Portella G, Passaro C, Chieffi P. Aurora B: a new prognostic marker and therapeutic target in cancer. Curr Med Chem. 2011;18:482-96.

25. Tong T, Zhong Y, Kong J, Dong L, Song Y, Fu M, et al. Overexpression of Aurora-A contributes to malignant development of human esophageal squamous cell carcinoma. Clin Cancer Res. 2004;10:7304-10.

26. Steeghs N, Eskens FA, Gelderblom H, Verweij J, Nortier JW, Ouwerkerk J, et al. Phase I pharmacokinetic and pharmacodynamic study of the aurora kinase inhibitor danusertib in patients with advanced or metastatic solid tumors. J Clin Oncol. 2009;27:5094-101.

27. PHA-739358 for treatment of hormone refractory prostate cancer. ClinicalTrials gov Identifier: NCT00766324. 2007.

28. PHA-739358 in treating patients with chronic myelogenous leukemia that re- lapsed after imatinib mesylate or c-ABL therapy. ClinicalTrialsgov Identifier: NCT00335868. 2007.

29. Steeghs N, Mathijssen RH, Wessels JA, de Graan AJ, van der Straaten T, Mariani M, et al. Influence of pharmacogenetic variability on the pharmacokinetics and toxicity of the aurora kinase inhibitor danusertib. Invest New Drugs. 2010.

30. Paquette R, Shah N, Sawyers C, Martinelli G, John N, Chalukya M, et al. PHA-739358, an Aurora kinase inhibitor, induces clinical responses in chronic myeloid leukemia har- boring T315I mutations of BCR-ABL. Blood. 2007;110 (11, Pt 1).

31. Fidler IJ, Kim SJ, Langley RR. The role of the organ microenvironment in the biology and therapy of cancer metastasis. J Cell Biochem. 2007;101:927-36.

32. Lin YG, Immaneni A, Merritt WM, Mangala LS, Kim SW, Shahzad MM, et al. Targeting aurora kinase with MK-0457 inhibits ovarian cancer growth. Clin Cancer Res. 2008;14:5437-46.

33. Stelter L, Amthauer H, Rexin A, Pinkernelle J, Schulz P, Michel R, et al. An orthotopic model of pancreatic somatostatin receptor (SSTR)-positive tumors allows bimodal imaging studies using 3T MRI and animal PET-based molecular imaging of SSTR expression. Neuroendocrinology. 2008;87:233-42.

34. Benten D, Follenzi A, Bhargava KK, Kumaran V, Palestro CJ, Gupta S. Hepatic targeting of transplanted liver sinusoidal endothelial cells in intact mice. Hepatology. 2005;42:140-8.

35. Kerbel RS. What is the optimal rodent model for anti-tumor drug testing? Cancer Metastasis Rev. 1998;17:301-4.

36. von Wichert G, Jehle PM, Hoeflich A, Koschnick S, Dralle H, Wolf E, et al. Insulin-like growth factor-I is an autocrine regulator of chromogranin A secretion and growth in human neuroendocrine tumor cells. Cancer Res. 2000;60:4573-81.

37. Weber K, Thomaschewski M, Warlich M, Volz T, Cornils K, Niebuhr B, et al. RGB marking facilitates multicolor clonal cell tracking. Nat Med. 2011;17:504-9.

38. Arnold R, Wilke A, Rinke A, Mayer C, Kann PH, Klose KJ, et al. Plasma chromogranin A as marker for survival in patients with metastatic endocrine gastroenteropancreatic tumors. Clin Gastroenterol Hepatol. 2008;6:820-7.

39. Baudin E, Gigliotti A, Ducreux M, Ropers J, Comoy E, Sabourin JC, et al. Neuron-specific enolase and chromogranin A as markers of neuroendocrine tumours. Br J Cancer. 1998;78:1102-7.

40. Peracchi M, Conte D, Gebbia C, Penati C, Pizzinelli S, Arosio M, et al. Plasma chromogranin A in patients with sporadic gastro-entero-pancreatic neuroendocrine tumors or multiple endocrine neoplasia type 1. Eur J Endocrinol. 2003;148:39-43.

41. Ramage JK, Davies AH, Ardill J, Bax N, Caplin M, Grossman A, et al. Guidelines for the management of gastroenteropancreatic neuroendocrine (including carcinoid) tumours. Gut. 2005;54 Suppl 4:iv1-16.

42. Zatelli MC, Torta M, Leon A, Ambrosio MR, Gion M, Tomassetti P, et al. Chromogranin A as a marker of neuroendocrine neoplasia: an Italian Multicenter Study. Endocr Relat Cancer. 2007;14:473-82.

Table 1: Expression of aurora kinases and phospho-H3S10 in human GEP-NETs

Localization	Grading	Ki-67 (%)	Aurora A	Aurora B	Phospho-H3S10
Pancreas	G1	<2%	+	-	-
Pancreas	G1	<2%	+	-	-
Pancreas	G1	<2%	++	++	+
Pancreas	G1	1%	+	-	-
Pancreas	G1	n.a.	+	-	-
Pancreas	G1	1%	+	-	-
Pancreas	G1	n.a.	+	-	-
Pancreas	G1	n.a.	++	-	-
Pancreas	G2	>2%	+	-	+
Pancreas	G2	>2%	++	-	-
Pancreas	G2	n.a.	++	-	-
Pancreas	G2	5%	+	-	-
Pancreas	G3	>20%	++	+	+
Small bowel (Ileum)	G1	<2%	+	+	-
Small bowel (Duodenum)	G1	n.a.	++	-	-
Small bowel (Ileum)	G1	<2%	+++	-	-
Small bowel (Ileum)	G1	1%	-	-	-
Small bowel (Ileum)	G1	<2%	+	-	-
Small bowel (Ileum)	G1	<2%	+	-	-
Small bowel (Ileum)	G1	<2%	+++	+	+
Small bowel (Ileum)	G1	<2%	+	-	-
Small bowel (Ileum)	G1	n.a.	+	-	-
Small bowel (Ileum)	G1	n.a.	+	-	-
Small bowel (Ileum)	G1	n.a.	++	-	-
Small bowel (Ileum)	G1	1%	+	-	-
Small bowel (Ileum)	G1	<2%	+	-	-
Small bowel (Ileum)	G1	n.a.	++	-	-
Small bowel (Ileum)	G1	n.a.	+	-	-
Small bowel (Ileum)	G1	n.a.	++	-	-
Small bowel (Jejunum)	G1	n.a.	++	-	-
Small bowel (Ileum)	G1	1%	++	-	-
Small bowel (Ileum)	G2	>2%	+	+	+
Small bowel (Ileum)	G2	5%	+	-	-

n.a., not available

Table 2: Effects of therapy with danusertib on the growth of subcutaneous human GEP-NET xenografts in NOD/SCID mice.

Experiment	**Number**	**Initial (mm^3) mean±SD**	**Final (mm^3) mean±SD**	**Final (% growth) median±SD**
BON1				
Control	45	52.3 ± 22.6	356.9 ± 224.6	627.2 ± 395.4
STZ/5-FU	29	44.7 ± 19.8	121.1 ± 72.7[a]	238.4 ± 194.3[a]
Danusertib	35	47.7 ± 22.4	42.0 ± 332.5[a,b]	73.9 ± 79.9[a,b]
QGP				
Control	35	49.5 ± 26.2	280.9 ± 205.6	436.3 ± 259.5
STZ/5-FU	25	54.2 ± 23.9	75.3 ± 51.2[a]	130.7 ± 86.2[a]
Danusertib	22	45.8 ± 24.3	4.6 ± 9.2[a,b]	6.3 ± 8.2[a,b]

[a]P<0.001 vs. controls, [b]P<0.001 vs. STZ/5-FU.

Table 3: Effects of danusertib treatment on BON1 and QGP liver metastasis in the orthotopic tumor model.

Experiment	**Number**	**Initial (mm^3) mean±SD**	**Final (mm^3) mean±SD**	**Final (% growth) median±SD**
BON1				
Control	10	2.9 ± 1.3	55.9 ± 39.7	1495.3 ± 1277.9
Danusertib	10	2.8 ± 1.4	5.2 ± 3.8[a]	164.5 ± 50.2[a]
QGP				
Control	5	7.5 ± 4.2	51.7 ± 35.0	810.7 ± 355.4
Danusertib	4	5.8 ± 3.4	6.1 ± 4.3[b]	108.7 ± 58.9[a]

[a]P<0.01 vs. controls, [b] P<0.05 vs. controls

Figure Legends

Figure 1: Aurora kinase expression in human GEP-NET tissues and cells. (A-B) Immunohistochemistry of a G1 midgut NET with nuclear and cytoplasmatic aurora-A expression (A) and aurora-B expression in two nuclei (B, arrows) one of which showing a mitotic figure. (C) Western blot after differential cell lysis with aurora-A and aurora-B expression in nuclei and cytoplasms of human GEP-NET cell lines BON1 and QGP. (D-E) Immunohistochemistry of subcutaneous BON1 xenograft tumor with expression of aurora A (D) and aurora B (E) in vivo. (F) Positive immunostaining for pH3S10 indicating aurora-B activity in BON1 xenograft tumors. Magnification: A, B, D, E x400; F x200

Figure 2: Effects of danusertib treatment in vitro. (A-B) Effects of danusertib in rapidly proliferating BON1 (A) and moderately proliferating QGP cells (B). Significant antiproliferative effects of danusertib were seen at 50nM and 500nM compared to DMSO-treated controls. (C) Cell cycle profile of BON1 cells mediated by danusertib after 48h at the indicated concentrations. Similar results were obtained in QGP cells (not shown). (D) Nuclear staining for pH3S10 and propidium iodide, exemplarily shown for BON1 cells with quantification by flow cytometry, 24h after treatment with 500nM danusertib. The gate indicates pH3S10 positive cells. (E) Effects of danusertib treatment for 24h on PARP-1 cleavage as an indicator of caspase mediated apoptosis. The 116kDa band indicates full length PARP-1; the 89kDa band represents the large PARP-1 fragment.

Figure 3: Subcutaneous GEP-NET xenograft model. (A-B) Danusertib treatment with 2x15 mg/kg/d effectively inhibits growth of BON1 (A) and QGP tumors (B) in vivo in comparison to controls and standard chemotherapy therapy with STZ/5-FU (1x15mg/kg/d). P-values <0.001 for danusertib treatment compared with controls from day 4 and compared with STZ/5-FU from day 12. (C) Serum levels of CgA in BON1 tumor bearing mice were significantly lower compared to

controls and mice treated with STZ/5-FU. p-values *p<0.001 compared with control, **p<0.05 compared with STZ/5-FU.

Figure 4: Biodistribution of GEP-NET cells after intrasplenic injection. (A) 2h after BON1 cell transplantation, human PCR signals were detectable almost exclusively in the liver. (B) Massive hepatomegaly with multiple tumor nodules, 5 weeks after intraportal BON1 cell transplantation. (C) Fluorescence in-situ hybridization using a digoxigenin-labled alphoid-DNA probe verifies human origin of GEP-NET liver metastases in mice. (D) Hematoxylin/Eosin staining showing nodular BON1 liver metastases (arrows), some with central necrosis (*N*). Magnification: C x400; D x100

Figure 5: Characterization of liver metastases from GEP-NET cells. (A) Strong expression of CgA in BON1 metastases in the mouse liver. (B-C) Immunohistochemistry for Ki-67 and PCNA of BON1 tumors revealed high proliferation of liver metastases. (E) Hematoxylin/Eosin-Staining of QGP metastases showing typical NET morphology. (E) Human origin of CgA-negative QGP metastases was verified by in-situ-hybridization. (F) Immunohistochemistry using mouse specific anti-CD31 showed that capillary vessels (arrows) in human GEP-NET metastases were of murine origin. Magnification: A x40; B x100; C, D, F x200, E x400

Figure 6: Treatment of orthotopic GEP-NET liver metastases with danusertib. Serial MRIs of mice bearing GEP-NET liver metastases demonstrated different growth pattern of BON1 (A) versus QGP metastases in the liver (B). Danusertib treatment inhibited growth of liver metastases derived from both human GEP-NET cell lines (C): BON1 (left panel; n=10 vs. n=10 controls) and QGP (right panel; n=4 vs. n=5 controls). Box plots indicating median, upper and lower quartiles, as well as lowest and highest observation. Danusertib 2x15mg/kg (white bars) was well tolerated and significantly suppressed tumor growth compared to vehicle treated controls (grey bars). Day 12: p<0.01 BON-1 compared with control, p<0.05 QGP compared with controls.

Figure 1

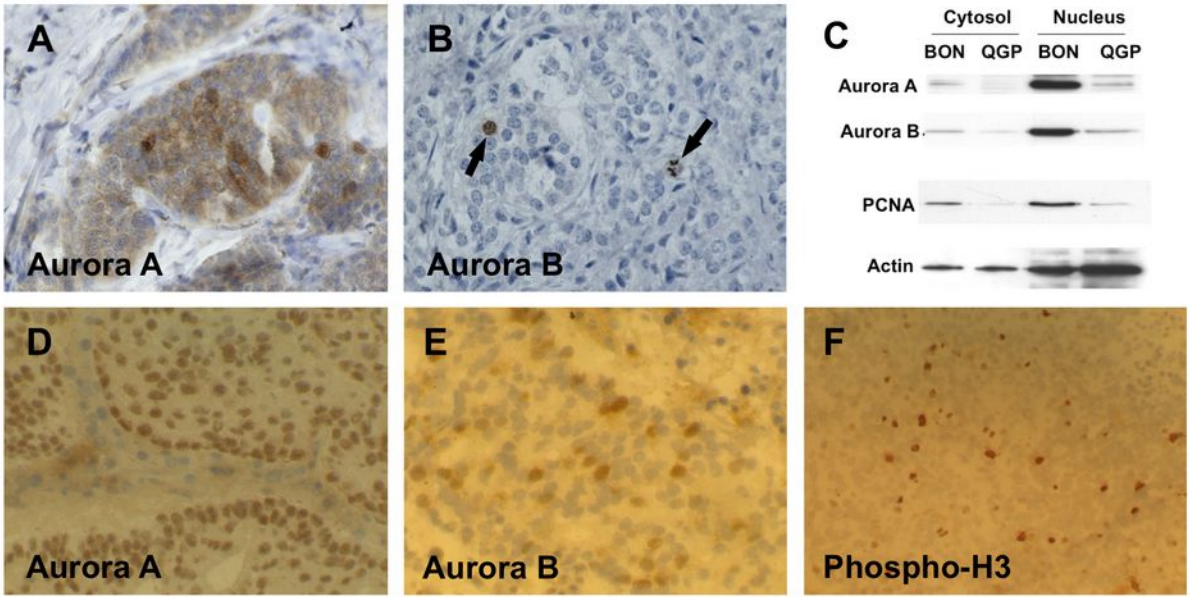

Figure 2

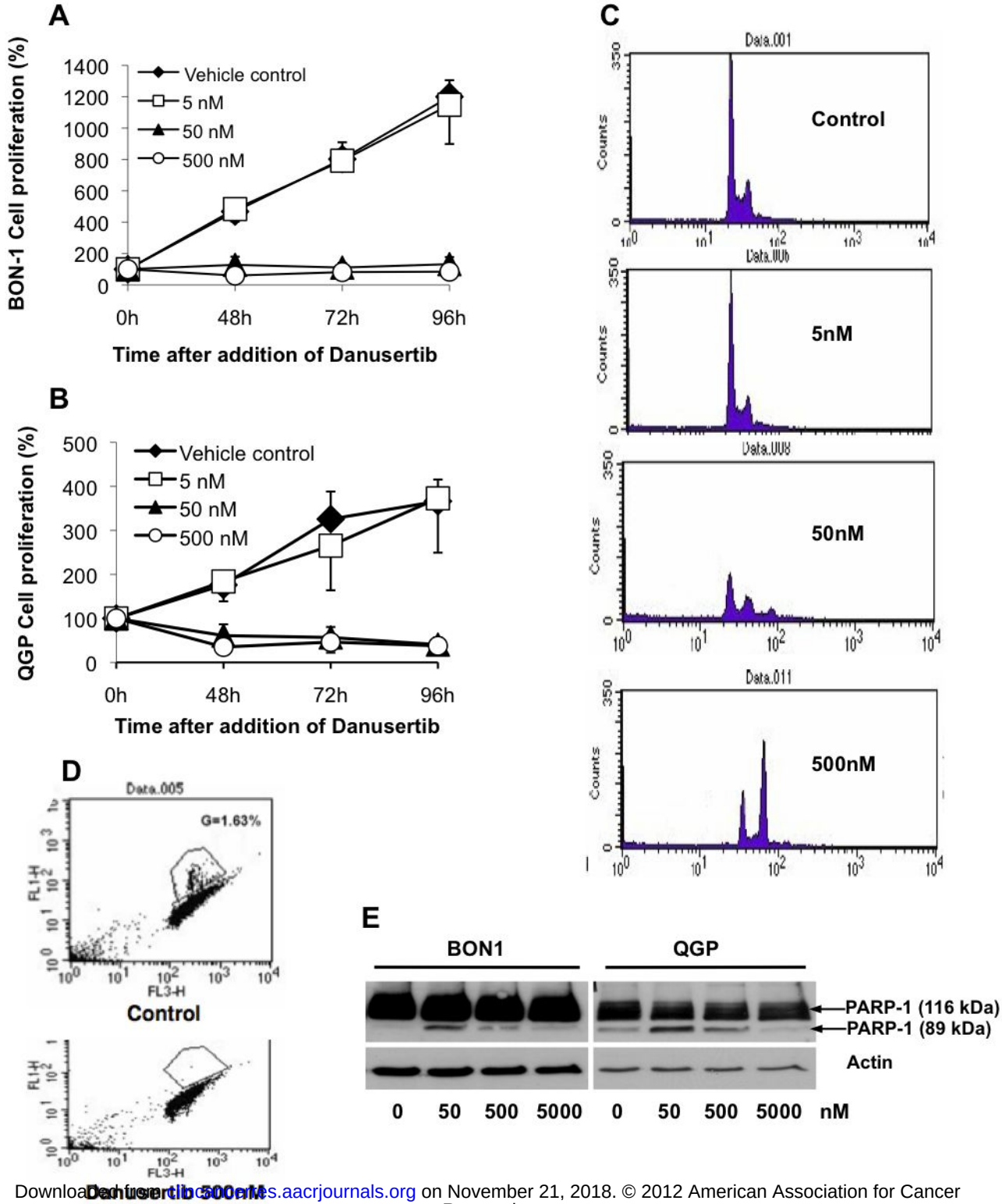

Figure 3

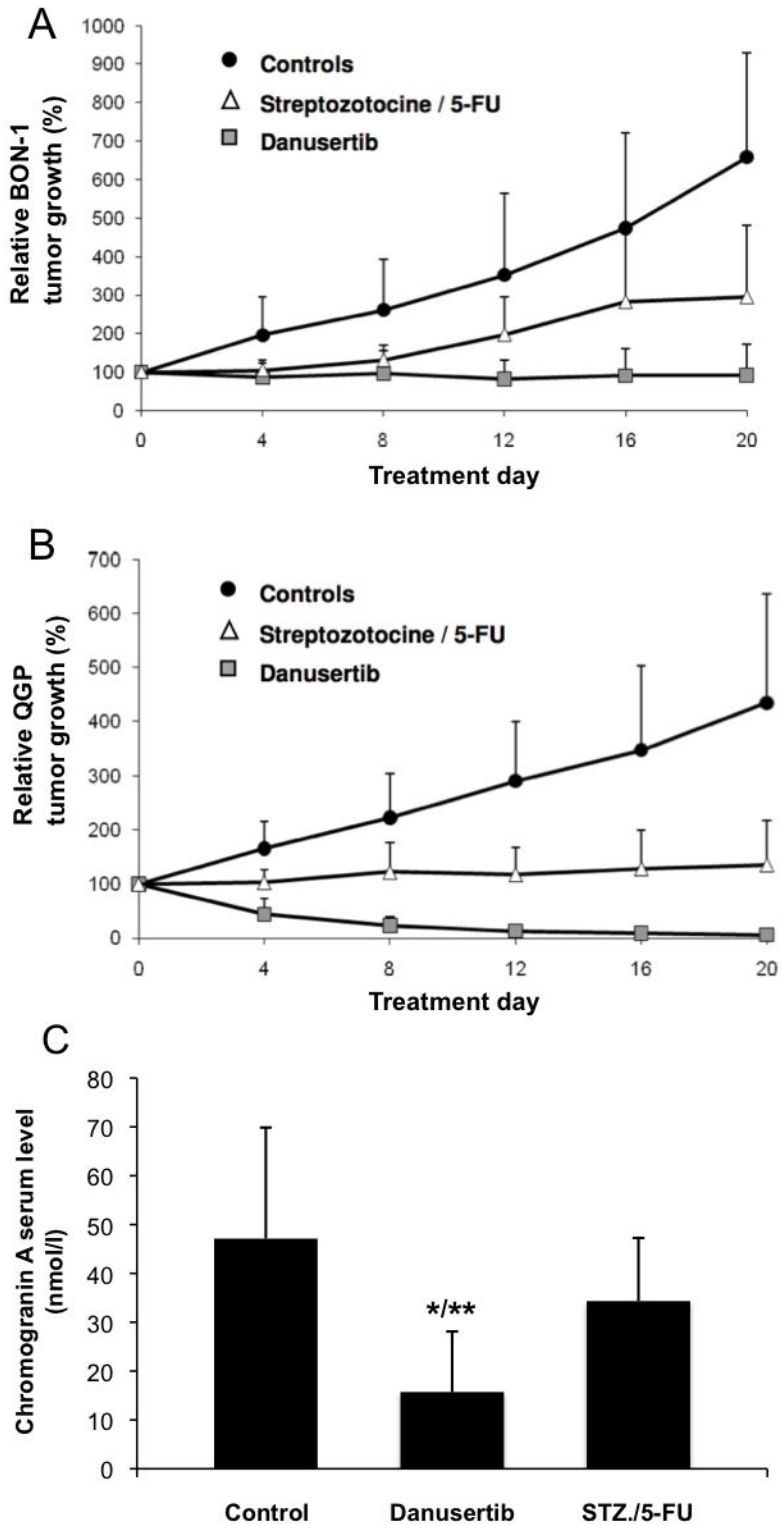

Figure 4

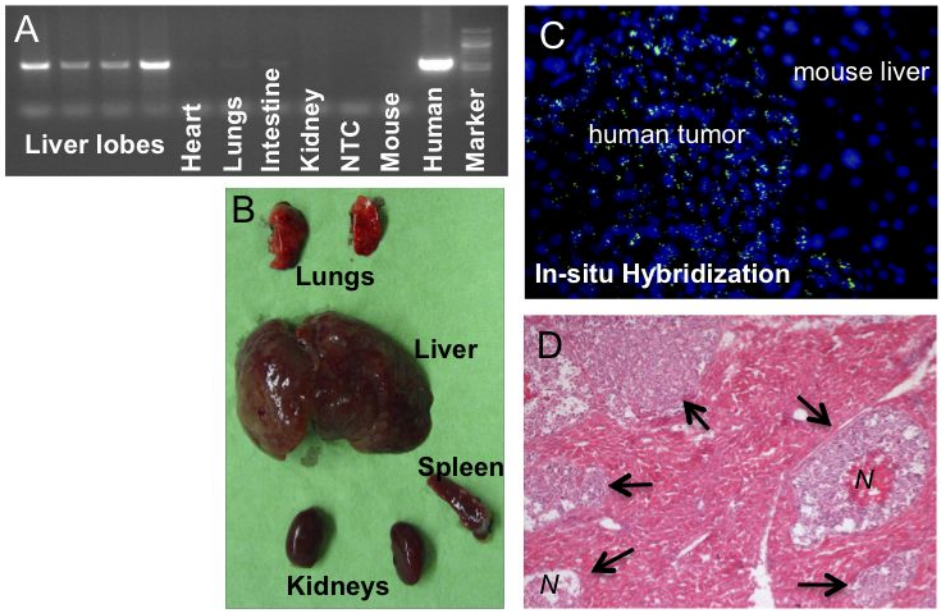

Figure 5

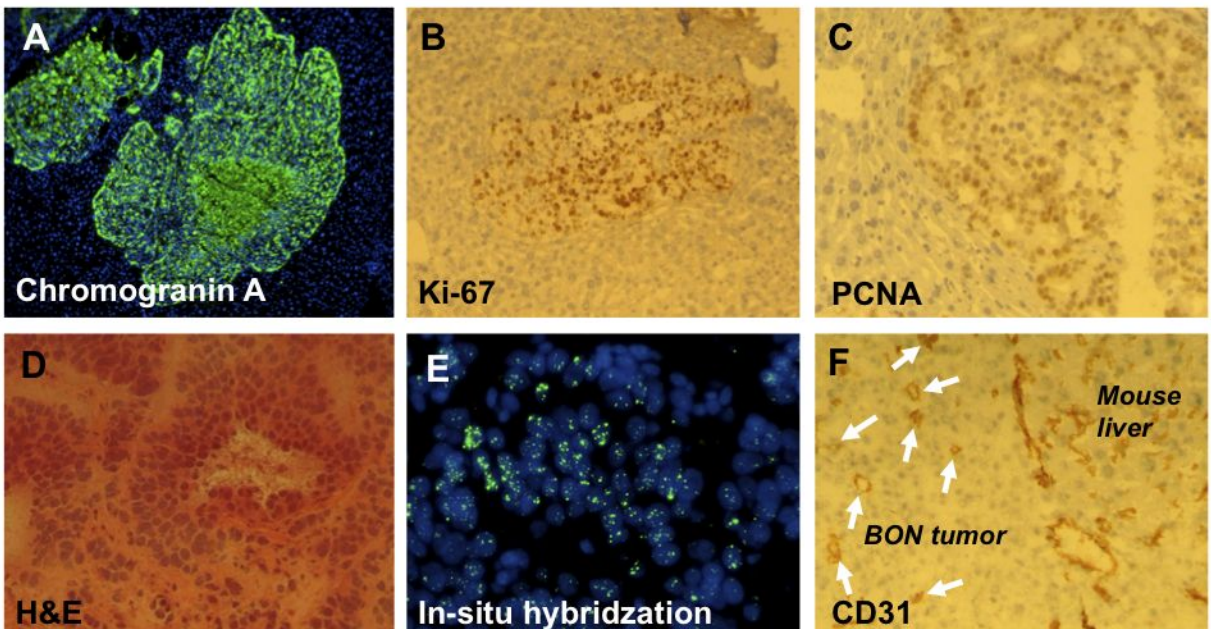

Figure 6

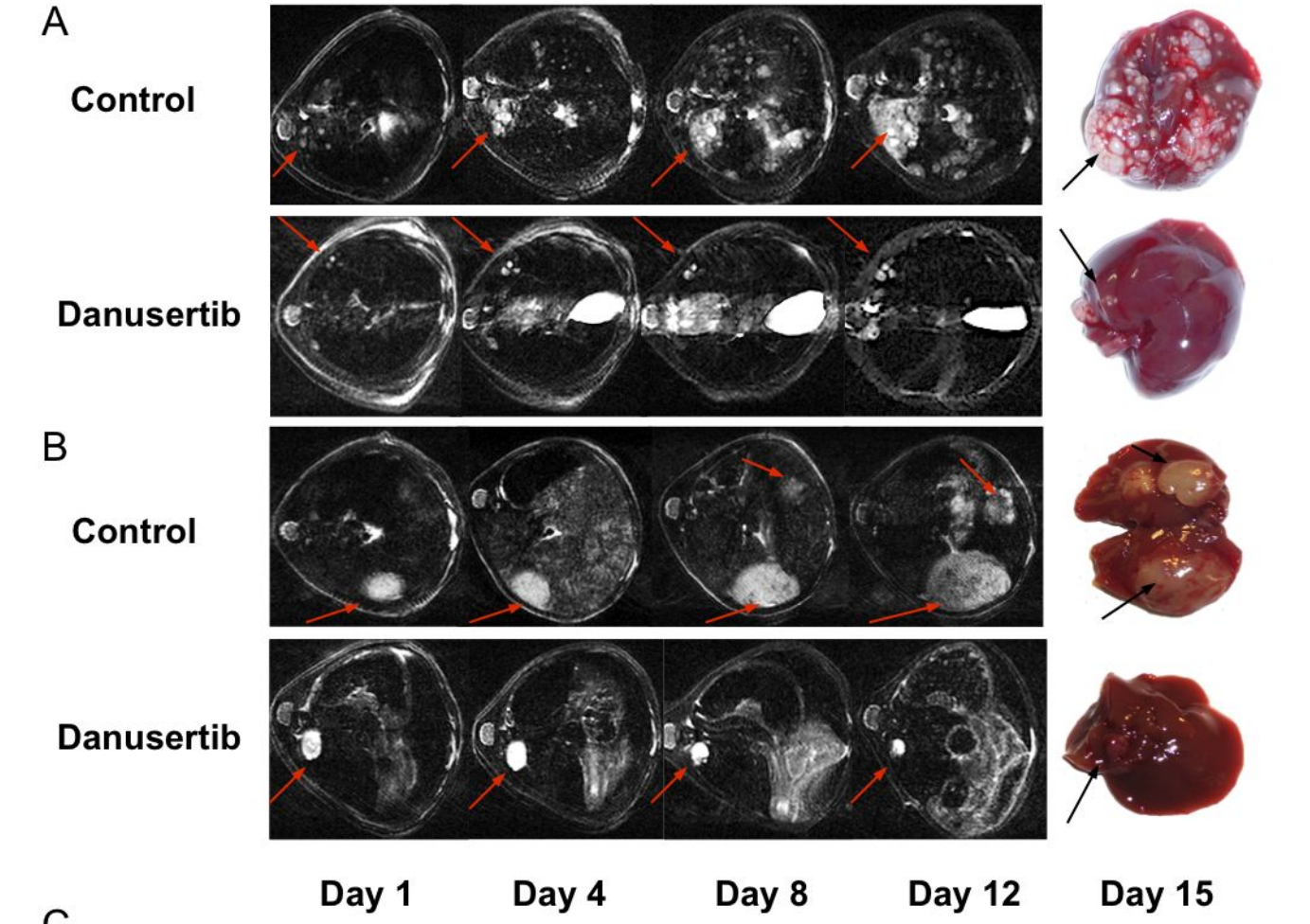

AACR American Association for Cancer Research

Clinical Cancer Research

Targeting aurora kinases with danusertib inhibits growth of liver metastases from gastroenteropancreatic neuroendocrine tumors in an orthotopic xenograft model

Katharina Fraedrich, Jörg Schrader, Harald Ittrich, et al.

Clin Cancer Res Published OnlineFirst July 2, 2012.